Intermediate Layers responses to Geomagnetic Activity During the 2009 Deep Solar Minimum Over the Brazilian Low Latitude Sector.

A. M. Santos[1], C. G. M. Brum[2], I. S. Batista[1], J.H.A. Sobral[1], M. A. Abdu[1], and J. R. Souza[1]

[1]National Institute for Space Research, São José dos Campos, Brazil.

[2]Arecibo Observatory, University of Central Florida, Arecibo, Puerto Rico.

Corresponding author: Ângela Santos (angelamacsantos@gmail.com; angelasantos_1@yahoo.com.br)

Key Points:

- A small variation in the geomagnetic activity during low solar activity can affect the *ILs* over Cachoeira Paulista.
- An overshielding electric field can cause a downward movement of the *ILs* in the early morning.
- During daytime, the smoothed rise of the *ILs* can be related to the regular undisturbed day-to-day zonal electric field of the ionosphere.

Abstract

Intermediate layers (*ILs*) are regions of enhanced electron density located in the ionospheric valley that extends from the peak altitude of the daytime E-region to the bottom side of the F-region. This work presents the daytime behavior of the ILs parameters (the virtual height - *h'IL*, and the top frequency - *ftIL*) for the deepest solar minimum of the last 500 years. In such a unique condition, this research reveals for the first time the *ILs*' quiet state seasonal behavior as well as its responses to moderate changes in the geomagnetic activity. Among the finds, it is highlight the annual periodicity of the *ftIL* while the *h'IL* presents semiannual component. The results also show that even small variations of geomagnetic activity (quantified by the planetary Kp index) are able to modify the dynamics of the *ILs* parameters. For the first time, it was observed that during December solstice and September equinox, the *h'IL*/*ftIL* decrease/increase rapidly with the increase of geomagnetic activity at the beginning of the day. As the day progresses, smoothed rise in the *h'IL* is observed at the same time in which a considerable decrease in the *ftIL* occurs, except during June solstice when a different behavior is observed both in relation to the annual as the seasonal average values of the *ftIL*.

1. Introduction.

The deep solar minimum of the solar cycle 23/24 provides an unprecedented opportunity to understand the variability of Earth's ambient ionosphere. During this period, an unusually inactive state of the sun with only relatively small sunspot-carrying active regions was observed. The solar fluxes (UV, EUV, and X-rays) responsible for the heating of the upper atmosphere and production of the ionosphere and the well-known 10.7 cm solar radio flux (F10.7cm) presented very low values when compared to the previous solar cycle (see for example Balan et al. 2012 and Kutiev et al. 2013). This period was considered the deepest solar minimum of the last 500 years (Hady, 2013).

Echer et al. (2012) reported an extremely low geomagnetic activity during the deep solar cycle minimum of 2008-2009. They investigated the long term variation of the solar wind and the geomagnetic parameters and found that the sunspot number, the interplanetary magnetic field (IMF) magnitude Bo, and the solar wind speed presented the lowest values during the space era. Additionally, they observed that the variance of the IMF southward Bz component was low. These exceedingly low solar wind parameters made the energy transfer from the solar wind to the magnetosphere minimal and the geomagnetic activity (quantified by the ap index in the referred work) reached extremely low levels. Zerbo et al. (2013) mentioned that the lowest solar activity and geomagnetic activity, since 1901, were registered in 2009.

Some studies have been carried out in order to understand the behavior of the equatorial and low latitudes ionosphere during the geomagnetic storm events in this very special period. Liu et al. (2012), for example, discussed the impacts of the high-speed stream in the equatorial ionization anomaly (EIA) development. Using the Digisonde data over Jicamarca and GPS data over the American meridional sector during 5-7 January 2008, they showed inhibition in the EIA formation probably due to a westward disturbance dynamo electric field. In this case, it was observed that the critical frequency of the F layer (f_oF2) increased and its peak height (hmF_2) decreased over the equatorial region. Such changes were observed during a reversal of the eastward equatorial electrojet (EEJ) to westward. Additionally, a prominent 9-day oscillation in hmF_2 and foF_2 over the equator was observed during the year of 2008. Liu et al. (2012) also found the same periodicity in the equatorial F region vertical drifts data obtained from the Fejer and Scherliess's (1997) empirical model. This model describes the storm-time vertical drift perturbations due to the combined effects of the prompt penetration electric field (PPEF) and the disturbance dynamo electric field (DDEF) as a function of the AE index. In agreement with the results presented by Liu et al. (2012), the 9-day oscillation was clearly present in the drift related to the DDEF but absent in the drifts related to PPEF. However, the DDEF effects alone are not sufficient to explain the observed phenomena. Other mechanisms, such as thermal expansion/contraction and neutral composition changes, are also needed to account for the periodic oscillation in the equatorial ionosphere (Liu et al. 2012).

The impacts of a weak geomagnetic storm that occurred in June 2008, on the F region zonal and vertical plasma drifts, over the equatorial station of Jicamarca was studied by Santos et al. (2016). A perfect anti correlation between the vertical and the zonal drifts close to the evening prereversal enhancement of the zonal electric field was

observed in the initial and growth phases of the magnetic storm. Based on a realistic low-latitude ionospheric model (SUPIM - Sheffield University Plasmasphere-Ionosphere Model), it was shown that this anticorrelation was driven mainly by a vertical Hall electric field induced by the primary zonal electric field in the presence of an enhanced nighttime E region ionization (see Abdu et al.,1998). The increase in the field line-integrated Hall-to-Pedersen conductivity ratio due to precipitation of energetic particles in the region of the South American Magnetic Anomaly was necessary to explain the observed anticorrelation between the vertical and zonal plasma drifts.

Sreeja et al. (2011) studied the impacts of a dusk-to-dawn penetration electric field in the daytime ionospheric east-west drift velocities during the storm main phase of the moderate geomagnetic storm of 21–25 July 2009. This event was considered anomalous because the storm main phase developed during northward orientation of the IMF. It was verified that during the reversal of the Bz to northward, the daytime E-region westward drift over Trivandrum (8.5°N, 77°E; dip latitude ~0.5°N) presented a reduction that was simultaneous with the disappearance of the equatorial sporadic E layer (E_{sq}) echoes in the ionograms. It was suggested that an additional overshielding electric field (westward/eastward during the day/night), superposed on the ionosphere during the storm main phase contributed to the observed reduction in the drift.

While there are many works that investigated the effects of the geomagnetic storms on the *E*, *F*, and sporadic-*E* (E_s) layers, little has been discussed about such effects on the ionospheric valley region or on the layers located between the upper *E* region and the *F* layer bottom-side, also known as intermediate layers (*ILs*), mainly over the equatorial and low latitude regions. Recently, the *ILs* over Brazil were studied and among many other features, it was found that these layers could suffer in some way the influence of the prompt penetration electric fields. Dos Santos et al. (2019), for example, reported a case in which a daytime *IL* over the equatorial region of São Luis on October 9, 2009 presented a strong upward movement that carried the *IL* to the base of the F_2 layer in ~ 1.5 hours. This anomalous rise was probably caused by the joint action of the atmospheric gravity wave propagation and the PPEF. Another interesting case of ascending *ILs* was presented by Santos et al. (2021), which occurred, however, during the sunset times. As mentioned by the authors, it is possible that the rise of the *IL* in these cases had been caused by the action of the PRE and in some events by an additional contribution from the prompt penetration electric fields. Among the seven cases studied (not all related to the magnetic storms), six occurred during a period of maximum solar activity and only one in 2009, which corresponded to a period of very low solar activity. In all the events, the *ILs* were located at altitudes higher than or equal to 175 km, except the event of November 10, 2003, when an E_s layer located at about 120 km of altitude presented an abrupt rise reaching 290 km of altitude in a time interval of ~ 1.25 hours. This rapid rise of the E_s/*IL* layers probably was caused by an eastward electric field of ~ 0.6 mV/m arising from the PRE and the PPEF (for more details, see Santos et al. 2021).

The focus of this paper is to investigate the geomagnetic activity effects on the intermediate layers over the Brazilian low latitude sector during the deep solar minimum of 2009. As mentioned previously, this epoch is especially suited to develop studies like the one proposed here due to the very low values of the solar decametric flux (10.7cm) that were observed. In this case, the effects caused in the *ILs* by the variability of radiation

coming from the Sun can be neglected, and consider only those caused by geomagnetic activity. A brief overview of the main characteristics of the intermediate layers over the Brazilian region is given in Section 2. The data sets and the results are presented in Section 3 and finally, in Section 4, the discussion and conclusions.

2. Intermediate Layers over equatorial and low latitudes regions over Brazil.

Intermediate layers (*ILs*) are regions of enhanced electron density located in the ionospheric valley that extends from the peak altitude of the daytime E-region to the bottom side of the F-region. Using the Digisonde data over the equator and low latitude regions over Brazil, dos Santos et al. (2019) and Santos et al. (2020; 2021) have studied the essential characteristics of the *ILs* during the minimum and the maximum solar activity epochs. It was observed that these layers are predominantly diurnal and present a typical downward movement that can last from minutes to hours. Depending on the height at which the *ILs* are formed, they can descend and merge with the normal ongoing sporadic -E (Es) layers. The *IL*'s occurrence over Brazil is high and seems to be dependent on the magnetic inclination angle and independent (or weakly dependent) on the solar activity. Nocturnal *ILs* also were observed over Brazil. Regarding the shape in which the *ILs* are seen in the ionograms, it was verified that they presented a curved format similar to the "h" type Es layer, however the *ILs* with a straight format and spreading base appearance also were observed.

The Digisonde routinely records ionograms at a cadence of 10 or 15 minutes, which makes it very difficult to track the precise origin of *ILs* and the exact moment when and how they were formed. However, dos Santos et al. (2019) also reported that in some cases, the *ILs* can be associated somehow with the F layer. Four situations were mentioned in which such characteristic could be observed, which are: (*a*) the intermediate layers are formed from the high-frequency end of the F1 layer; (*b*) the *ILs* are formed from a detachment of the F1 layer base; (*c*) the *ILs* are formed from a perturbation in the F2 layer base and, (d) the ascending *ILs* merge with the F layer base. Among these cases, the *IL*'s formation described in item (b) was very common over Brazilian region.

Regarding the *IL*'s lifetime, Santos et al. (2020) observed that over Brazil it is higher in solar minimum period (both over the equator and low latitude) and lower over the equator, independent of the solar activity. Over the equator, the *ILs* daily occurrence showed two maxima (at about 08:00 LT and 15:00 LT), both during the maximum and minimum solar activity epochs. Over low latitude, only one maximum was observed and it had higher amplitude during the low solar activity period. Similar to the equatorial region, the *ILs* occurrence was lower before midday and in the second part of the day, it was very similar in both periods.

The studies conducted so far on the *ILs* over Brazil give us some indications that the dynamics of these layers can be influenced by the atmospheric tides, gravity waves, and electric fields. The day-to-day variability in the average *ILs*' descent velocity also suggests the influence of a periodic perturbation with a periodicity of some days. The velocity values found are compatible with those of the semidiurnal and quarter-diurnal tides. However, the larger descending rate (> 10 km/h) observed over the equatorial region may reveal an additional influence of the gravity waves in *IL*'s dynamics. As

mentioned previously, Santos et al. (2021) reported interesting events in which the *ILs* presented an upward movement at the same time in which the F layer rises due to the evening prereversal enhancement of the zonal electric field. Such characteristic was observed in most of the cases during a period of high solar activity, between October and April months, however a single case also was observed in 2009. Therefore, it is possible that the more intense zonal electric field in 2003 could have an important contribution in the upward movement of the *ILs*.

3. Data sets and Results.

In this paper, the ionospheric sounding data collected by the Digisonde operated over the low latitude site, Cachoeira Paulista (CP, 22.42° S; 45° W, I: -34.4°), during the deep solar minimum of 2009 are used to verify the possible dependence of the *ILs* on the geomagnetic activity. The *ILs*' virtual height (*h'IL*) and top frequency (*ftIL*) are analyzed as a function of the Kp index. The *ILs* data were processed using the SAO Explorer software (Reisnish, 1986). All the observed *ILs* were included in the analysis, regardless of their descending or ascending movement.

Figure 1 summarizes the geophysical condition of the data distribution according to the solar and geomagnetic activities based on the F10.7P index and Kp_{av} index, respectively. The F10.7P is a combination of the daily decimetric solar flux index (F10.7) and one more term (F10.7A), which corresponds to the average of the 81 previous days, thus F10.7P= (F10.7A + F10.7)/2 (given in Solar Flux Units (SFU); 1 SFU = 10^{-22}W/(m^{2}Hz)). F10.7P was chosen because several authors have shown that the ionospheric parameters are better described by this index (Brum et al., 2011, 2012; Goncharenko et al., 2013). In fact, Brum et al. (2011) and Brum et al. (2012) have shown that the best description of the UV-EUV (based on UV-EUV irradiance data from Pioneer Venus Orbiter (10–150 nm) and by the Solar EUV Monitor onboard the Solar Heliospheric Observatory (26–34 nm and 0.1–50 nm bands)) is given by F10.7P when compared with F10.7. In addition, their works have shown that the UV-EUV emissions tend to increase with F10.7P until a certain threshold (around 175 SFU). However, for low solar activity, the UV-EUV variations with the F10.7P can be well represented by a linear function and this feature is very important for the methodology employed in this work, as seen below. The Kp_{av} is the average of the 3 hours data current Kp value and the previous 3 and 6 hours, that is, $Kp_{av} = (Kp_{(ref)} + Kp_{(ref-3)} + Kp_{(ref-6)})/3$, which gives the standard behavior of the geomagnetic activity and avoid sharp gradients in the temporal edges of this index (every 3 hours).

The occurrence number of the Kp_{av} level in this period is presented on the right bottom panel of Figure 1. It is observed that all of the data were acquired during very low to normal geomagnetic activity ($Kp_{av} \leq 3^+$ or 3.3) according to the Wrenn et al. (1987) classification. Such distribution is very similar to that found by Terra et al. (2020) when the authors analyzed the MSTID events for the period starting in the middle of 2018 to the end of 2019 (also low solar activity). Note that the occurrence of various levels of magnetic activity is well distributed throughout the year (left bottom panel of Figure 1) and this behavior is the optimum condition for the kind of analysis of this work, as will be seen in this report. Regarding the solar activity, the period that encompasses our data set is the end of the solar cycle #23 and the beginning of the solar cycle #24. A growth of

activity and fluctuations of F10.7P along the year, varying from 66.5 SFU to 78.1 SFU (average of 70.1, top right panel) and an uneven distribution of F10.7P (left upper panel) may be noted. This was a period of very low solar activity in terms of solar flux irradiance (see Emmert et al., 2010) and many works have reported unusual responses of the upper atmosphere/thermosphere under this condition. For instance, during this period, reduction of ionospheric temperatures and densities were detected over several latitudes (Coley et al., 2010; Heelis et al., 2009; Yue et al., 2010; Klenzing et al., 2011). Comparing the thermospheric total mass density from the prolonged minimum in solar activity between cycles 23 and 24 with that of the previous solar minima, Emmert et al. (2010) detected a reduction of about 10–30% compared with the climatologically expected levels. Heelis et al. (2009) and Aponte et al. (2013) reported an unprecedented contraction of the topside ionosphere to altitudes never reported before.

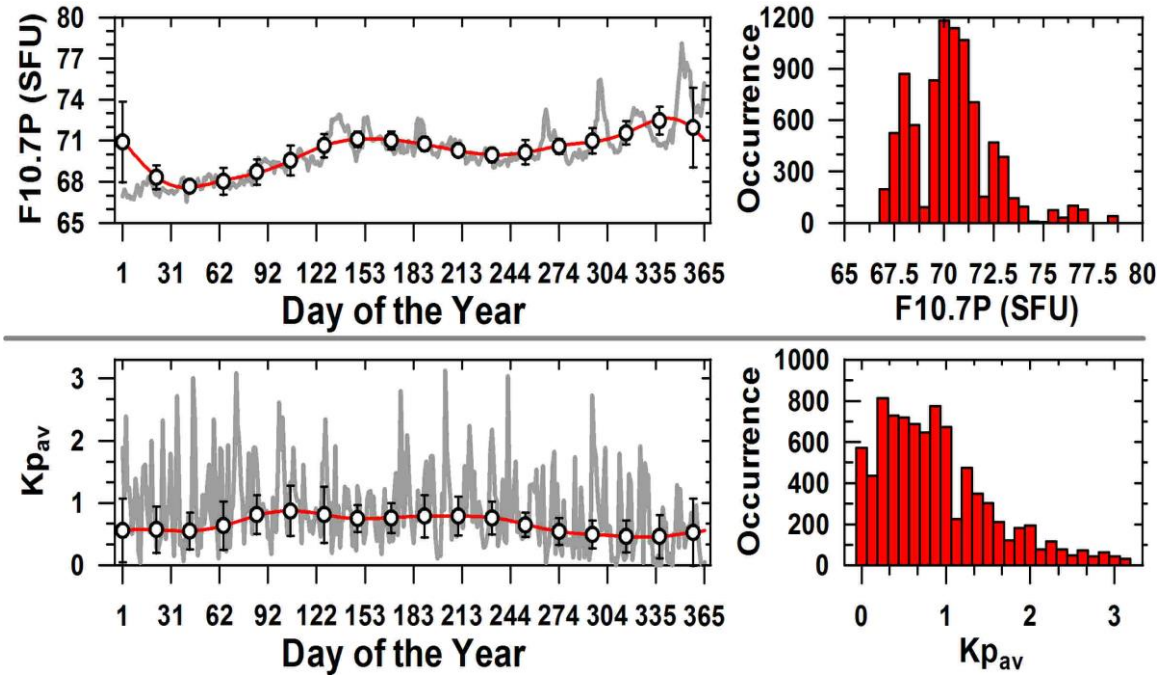

Figure 1. Variability of the solar and geomagnetic activity quantified by the F10.7P and the Kp_{av} indices (upper and bottom block of panels, respectively) for the studied period. Left panels show the geophysical conditions as a function of the day of the year while the right panels their corresponding number of occurrences. The dots of the left upper panel represent the 41 days averages and the standard deviation of F10.7P, while dots of the left bottom panel represent the same range of days of the upper panel and its respective standard deviation but for Kp_{av} <=2.3 (geomagnetic condition used to construct the quiet time condition of *h'IL* and *ftIL*). The red continuous lines are the reconstruction of theses variabilities using Fast Fourier Transform (FFT). The given occurrence in the right column of panels is the number of hours for a given interval of Kp_{av} (0.125) and F10.7P (0.5 SFU).

In our study, it has been used the *h'IL* and *ftIL* parameters as obtained from the Digisonde observation over Cachoeira Paulista for the year 2009. From these data, an empirical climatological model was developed that accounted for the dependences of these parameters on time and season, under low solar and geomagnetic activities. Determining the variability of *ILs*' parameters in function of time and season make it possible the isolation of any changes related to geomagnetic activity. The first step in our methodology was to extract the seasonal quiet time behavior of the *h'IL* and *ftIL*

parameters. For this, it was employed the weighted arithmetic mean defined as $x(t_{ref}, d)$ defined as (equation 1):

$$\bar{\boldsymbol{x}}(\boldsymbol{t_{ref}}, \boldsymbol{d_{ref}}) = \frac{\sum_{d=d_{ref}-20}^{d_{ref}+20} x(t_{ref},d)(|d_{ref}-d|)}{\sum_{d=d_{ref}-20}^{d_{ref}+20}(|d_{ref}-d|)}, \quad (1)$$

where $\boldsymbol{x}$ denotes *h'IL* or *ftIL* values under the geomagnetic activity below $Kp_{av} \leq 2.3$ for the time reference t_{ref} and the selected day of the year (DOY=*d*). The average value of height and frequency of the ILs was calculated considering 20 days adjacent to the $\boldsymbol{d_{ref}}$ and 30 minutes around the t_{ref} .

From the quiet time variability of the *h'IL* and *ftIL* obtained by the 40 days weighted arithmetic mean process a simple model was built using finite Fourier series reconstruction following the procedure by Souza et al. (2010) and Brum et al. (2011), as given by

$$\boldsymbol{xV(t,d) = A0(t) + 2\sum_{m=1}^{4}[A_m(t)cos(2\pi f_1 d) + B_m(t)sin(2\pi f_1 d)]}, \quad (2)$$

where $\boldsymbol{xV(t,d)}$ is the reconstructed variable as a function of time *(t)* in UT and DOY (*d*) ($\boldsymbol{xV}$ stands for *h'IL* or *ftIL*), $\boldsymbol{f_1}$ is the fundamental frequency of the parameter to be reconstructed (1/365), $\boldsymbol{A0(t)}$ is the annual average of the such parameter for a given *t*, and finally, $\boldsymbol{A_m(t)}$ and $\boldsymbol{B_m(t)}$ are the mth Fourier coefficients also as a function of time. The terms $\boldsymbol{A0(t)}$, $\boldsymbol{A_m(t)}$ **and** $\boldsymbol{B_m(t)}$ were incorporated to the model using a polynomial fitting in function of time (UT), as shown in Figure 2, for the harmonics m=1 (one year), m=2 (~6 months), m=3 (~4 months) and m=4 (~3 months). The upper left (*h'IL*) and right (*ftIL*) panels show the time dependence of $\boldsymbol{A0}$ (open circles for Fourier coefficients and continuous lines for adjustments). The values of $\boldsymbol{A_m}$ and $\boldsymbol{B_m}$ are presented in the lower right and left panels by the blue and red curves, respectively. The same as for the top panels, the open circles are the Fourier's harmonics and the solid lines represent their curves reconstructed by polynomial adjustments.

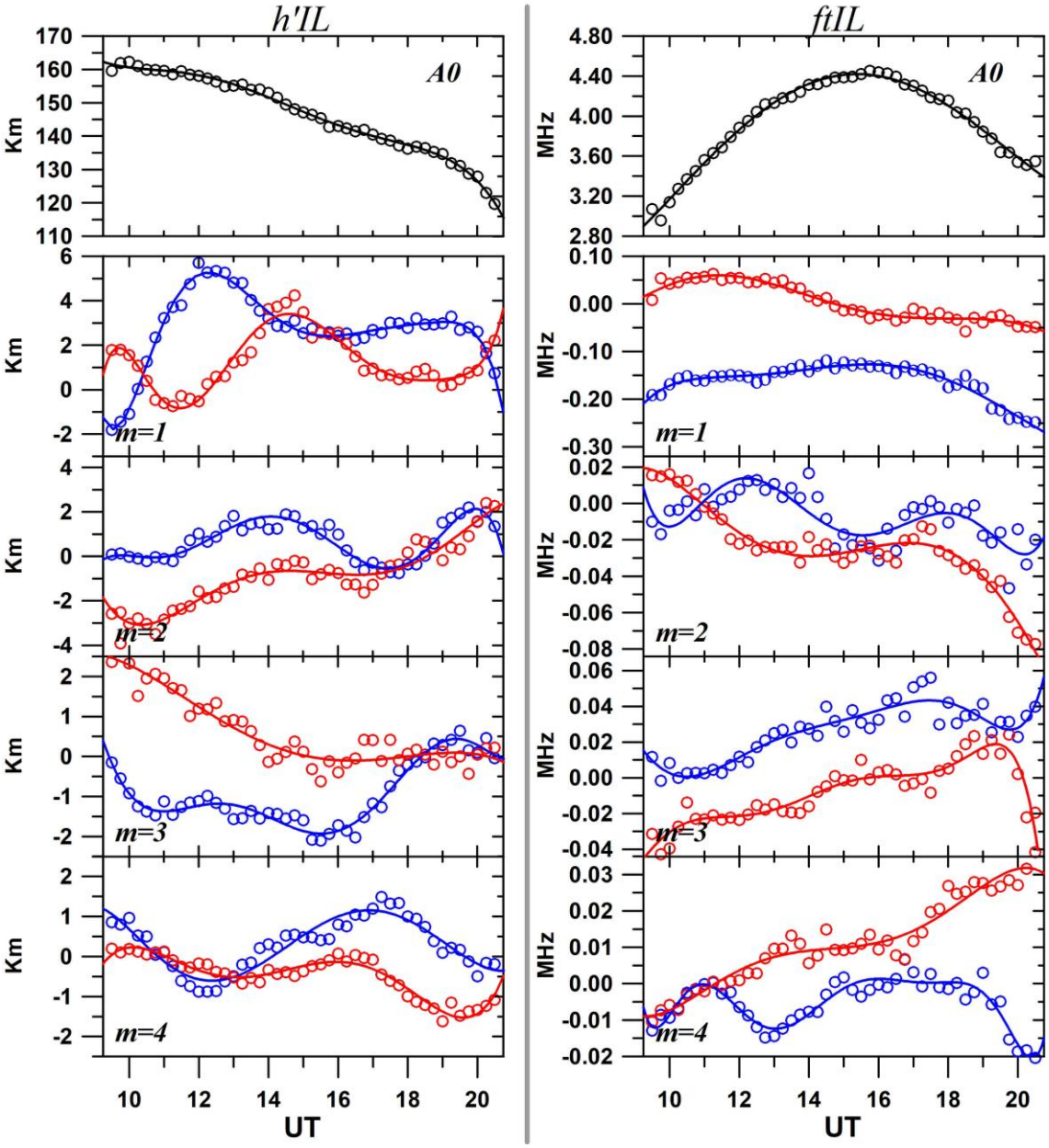

Figure 2. Dependence of the *h'IL*/*ftIL*'s FFT coefficients as a function of UT (left/right, respectively). The circles are the values obtained by the FFT decomposition, while the continuous lines are the best polynomial approximation (more information in the manuscript body).

Based on the model output above described, Figure 3 shows the behavior of the *h'IL* and *ftIL* during the year from 10:00 to 20:00 UT (top and bottom panel, respectively). The right panels show the dispersion diagram between the model and data (under Kp_{av}<=2.3) wherein it is possible to see the good correlation between the observation and the modeled data. The left panels show the semi-annual variation of the *ILs*' virtual height and top frequency an annual one. It can be verified that the upper intermediate layers (~ 180 km) are formed close to the winter solstice between 10:00 UT and 14:00 UT, with a maximum in April/May. A second maximum is observed in November/ December, however, in a more restricted range of time (from 10:00 UT to 12:00 UT). After 14:00 UT, the *ILs* are generally located at altitudes at or above to 140 km. It was observed in the ionograms (not shown here) that the upper *ILs* generally are formed very near to the *F1* layer base or apparently as the detachment of the *F1* layer. Some deformations can

occur in the *F1* and *F2* layer traces at the moments when these upper *ILs* are formed. In addition, it is observed that the evolution of the *ILs* to altitudes below 120 km was more evident between the months of April and May (DOY 92-153). In this case, the *ILs* probably merged with the Es-sporadic layers in development. The bottom left panel shows an annual variation of the top frequency, with a maximum at about 15:00-16:00 UT from November to February. It can be observed that the upper *ILs* present a lower frequency when compared to the layers located near to 140 km. As the *ILs* descend, they reach the *E* region and merge with the existing *Es* layer, increasing in this way, the top frequency of the layer due to the presence of the metallic ions.

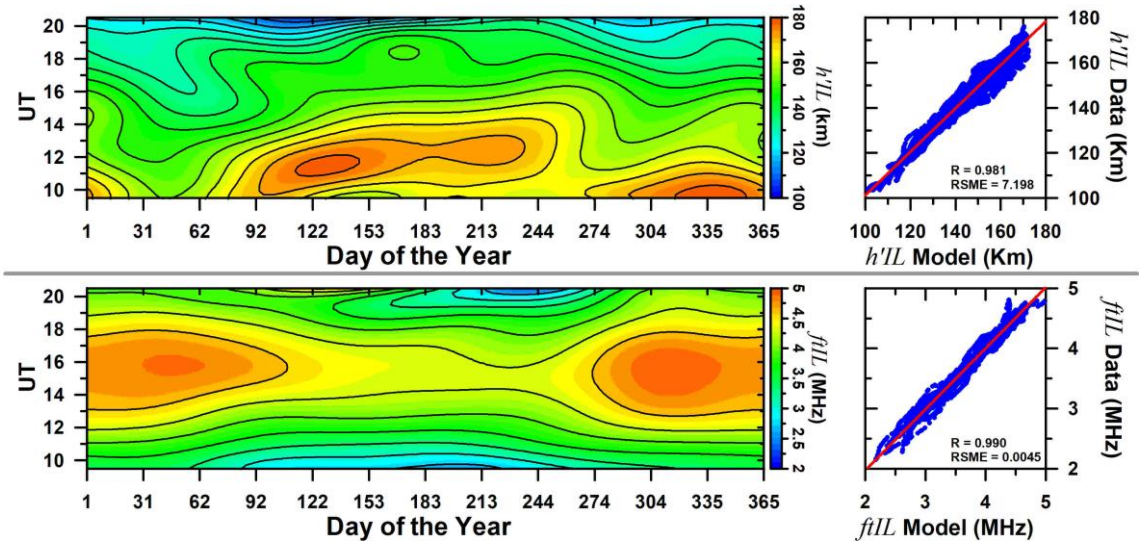

Figure 3. Contour plot of the annual variation of the modeled virtual height (*h'IL*, left top panel) and top frequency (*ftIL*, left bottom panel) of the intermediate layers over Cachoeira Paulista. The dispersion diagrams on the right hand side show the correlation between the observations and model results. In each panel on the right, the Correlation Coefficient (R) and Root Mean Square Error (RSME) values are also provided.

Figure 4 shows how the dependence of the different parameters of the intermediate layers in respect to geomagnetic activity was investigated in this work. The upper panel shows the whole data set sorted from the lowest to the highest Kp_{av} values and divided into eight sections with the same percentage of samples for each range of Kp_{av} (12.5%, represented by the black vertical lines) for the December solstice at 18:00 UT±30 minutes. Specifically, for this example, the selected range represents 366 data points, i.e., each 12.5% displays the behavior of ~45 individual data samples. This panel also displays the respective F10.7P values (red line) and its respective average and standard deviation (blue open circles) for the same sorted 12.5% occurrence range of Kp_{av}. Note that the F10.7P mean variation for each range does not vary much which leads us to emphasize that the following variations of *ILs* are due to geomagnetic activity. The bottom panels show the *h'IL* and *ftIL* responses to the geomagnetic activity by the residual average obtained by the difference of the registers and the model output presented in Figure 3 in function of ΔKp_{av}. The ΔKp_{av} is the mean of the respective Kp_{av} value minus the average of any value below Kp_{av} <=2.3 in a range of ±20 days (this is the geomagnetic condition that the model was developed, the red line shown in the left bottom panel of Figure 1). Noticed: The usage of the residuals minimizes the background quiet time behavior variation along the time, enhancing this way the detection of the real contribution or not of the geomagnetic

activity on the *IL*s parameters. The open circles represent the average values of the height/frequency residuals ($\Delta h'IL$ and $\Delta ftIL$, respectively) and ΔKp_{av} for the eight different levels of ΔKp_{av} and their respective standard deviations (vertical and horizontal lines). The linear fitting is indicated by the blue lines. The slope (SLP) of the dependence of *h'IL* and *ftIL* with respect to the geomagnetic activity variation (km. ΔKp^{-1} and MHz. ΔKp^{-1}) and the correlation factor (R) are also shown. In this example, it can be clearly observed that as the geomagnetic activity increase, the height of the intermediate layers also increases. The opposite occurs with the frequency when an increase of the Kp causes a decrease in this parameter.

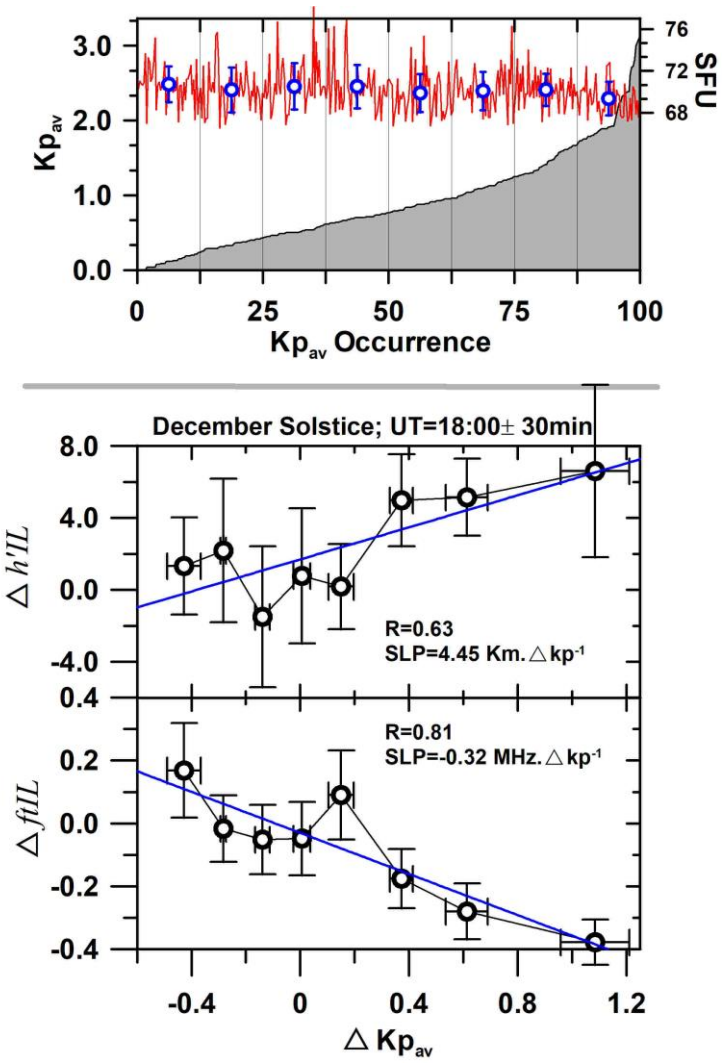

Figure 4. Responses of the intermediate layer to the geomagnetic activity for December Solstice at 18:00 UT±30 minutes. The upper panel shows the average Kp (Kp_{av}) data organized from the lowest to the highest values and divided into eight sections with the same percentage of samples for each range of Kp. In addition, the values of F10.7P with respect to Kp_{av} and the average of the F10.7P (blue open circles) for each section are also presented. The bottom panels show the linear regression over the height and frequency variability relative to the average Kp values.

The same methodology explained in the case of Figure 4 was applied to all the data between 09:00 and 21:00 UT for each season. Due to the lack of data, the night period was excluded from our analysis. In order to obtain the best statistical sampling, the occurrence rate was considered only in the cases in which it was possible to organize the

Kp_{av} levels in a minimum of six sections under the condition of the chosen cells (season and one hour). Figure 5 shows the *ILs*' dependence with the geomagnetic activity in terms of height (first two columns from left to right) and frequency (two columns of the middle) for different seasons. The data were grouped into ±40 days around the solstices and equinoxes of 2009 (December 21, March 20, June 21 and September 22). The fifth column shows the variation of the Kp_{av} index, that is, the difference between the higher and lower value of Kp_{av} observed in a given season for each time. The gray curve represents the annual average value of the *h'IL*, *ftIL* and $\Delta \boldsymbol{Kp_{av}}$. The correlation coefficient of these three parameters and their annual average are also shown. The number of days used in the averages values is indicated in the correlation coefficient panels by the red color. In order to get a good accuracy in our analysis only the data in which the correlation coefficient was higher than 0.5 was considered. It is observed that the higher variability in *ILs*' height with geomagnetic activity occurs at about 10:00 UT during the December solstice and September equinox. In this case the IL goes down fast with the increase of the geomagnetic activity. In the following hours, this descent decrease until a moment in which an opposite behavior occurs, that is, a small rise of the IL begins to be observed with the increase of the Kp_{av}. During March equinox, such characteristic is not observed. However, during all the interval analyzed, the rate values of km.ΔKp^{-1} was positive during the day, with a clear tendency of increase as the day goes on. It can be observed that during the June solstice, the behavior of the height with Kp_{av} was very similar to that of the annual average (gray curve). Regarding the behavior of the frequency, it is noticed that in the June solstice, the *ftIL* does not have a well-defined pattern, presenting an increase with the geomagnetic activity between 13:00 UT and 17:30 UT and a decrease after this (that is less pronounced when compared with the other seasons periods). Additionally, it is possible to verify that in the first hours of the day (between 10:00 UT and 13:00 UT in December solstice and 10:00 and 11:30 UT in September equinox) there is a tendency of this parameter to increase with the increase in geomagnetic activity. On the other hand, in the March equinox, the geomagnetic activity does not seem to cause any variation in *ftIL* between 10:00 UT and 11:00 UT. However, in the following hours, a well-defined decrease of the ILs' top frequency can be observed as the $\Delta \boldsymbol{Kp_{av}}$ increase. Such behavior is also evident in the December solstice after 13:00 UT. During September equinox, the same characteristic only can be observed in definitive after 16:00 UT, since before this the *ftIL* presents some moments of intensification and decrease with the increase in $\Delta \boldsymbol{Kp_{av}}$.

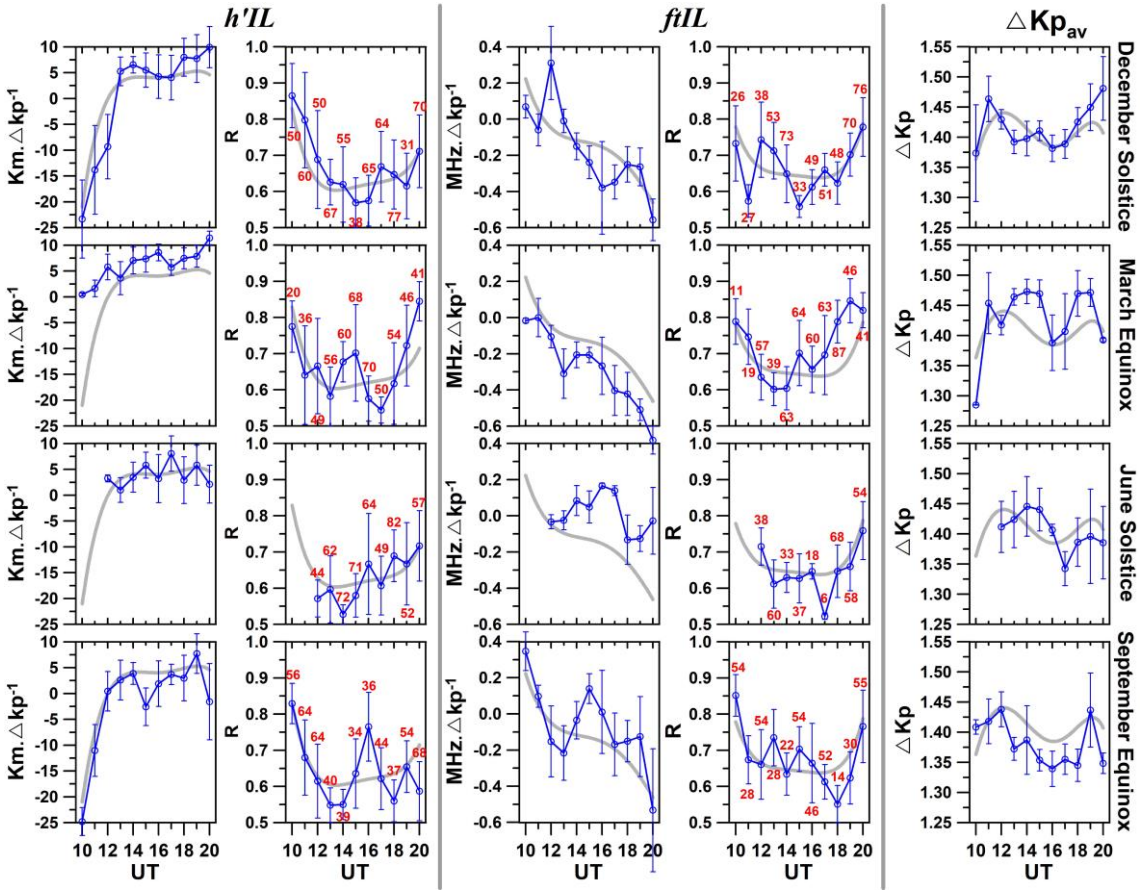

Figure 5. Geomagnetic activity effects on *h'IL* and *ftIL* parameters for different seasons. The first two panels (from left to right) show the linear regression of the *h'IL* as a function of the Kp index over the different times of the day and the correlation coefficient R. The middle panels indicate the same but for the *ftIL* parameter. The Kp_{av} variation is shown in the last panels (from top to bottom). The gray curve represents the annual averages of the *h'IL*, *ftIL*, and Kp index.

4. Discussion and Conclusions.

It is well known that geomagnetic activity can drastically modify the low-latitude ionospheric dynamics. During the last solar minimum, a unique opportunity was available to investigate such dynamics, since the effects of the solar activity, that dominates the temporal variability of ionospheric properties, could be practically disregarded due to very low solar activity. Using Digisonde data from the Brazilian low latitude station, Cachoeira Paulista, we studied the impacts of the geomagnetic activity in the height and top frequency of the intermediate layers during the deep solar minimum of 2009.

The results summarized in Figure 5 revealed, for the first time, that the most expressive response of the *ILs* over the low latitude region of Brazil to the geomagnetic activity occurred during the September equinox and the December solstice during the early morning hours (~ 10:00 UT/07:00 LT), when the *ILs* presented a trend of a rapid descent with the increase of the Kp_{av} (as indicated by the negative values of $\mathrm{km}.\Delta Kp^{-1}$ in *h'IL* panels). It is possible that this variation in the height of the *ILs* could have been caused by a disturbance electric field having the nature of an over-shielding electric field such as that associated with the northward IMF Bz turning. This electric field has westward polarity during daytime. As pointed out by Santos et al. (2021), depending on

the height at which the *ILs* are located, the disturbance electric field can affect considerably the vertical displacement of the intermediate layers. They showed that the eastward PPEF can affect partially the rises of the *ILs* located at higher altitudes (> 170 km) at sunset times. As shown in Figure 3 of the present work, the *ILs* were located at altitudes very close to this limit (> 165 km) between ~10:00 UT and 12:00 UT from October to January, reinforcing in this way the idea that a disturbance electric field could be responsible for the downward movement of the *ILs*.

Another interesting point that needs to be considered is that the movement of the *IL*s can also be influenced by the regular undisturbed day-to-day variations in the zonal electric field of the ionosphere that is directed to east/west during the daytime/nighttime hours. Therefore, it is possible that in the first 2-3 hours of our analysis period, the descent of the IL could be a result of a competition between the eastward zonal electric field created by the E-region dynamo and the disturbance westward electric field arising from the *overshielding* process. In the following hours, that is, after 12:00 UT or 13:00 UT, the layer descent presented a decrease until a moment in which an opposite situation was observed, that is, a small rise of the *ILs* occurred in all seasonal periods analyzed, as denoted by the positive values of the rate km.ΔKp^{-1} in the first panels on the left in Figure 5. In March equinox, this rise was more pronounced when compared to the other seasons as can be verified by the visual comparison between the respective slope of the curves from the different seasons (blue lines) and that of the annual average curve (gray line). A strong rise of the IL during daytime over the equatorial site of São Luis was reported by dos Santos et al. (2019). The authors mentioned that such upward movement of the IL might have been caused by the joint action of the gravity wave propagation and of the eastward PPEF. In the case studied by dos Santos et al. (2019), the rise of the IL also was accompanied by a decrease in their top frequency.

At the same time in which a decrease in the *ILs* height is observed, an increase in the *ftIL* parameter occurs. Taking, as an example, the September equinox, at about 10:00 UT the rate variation of the *ftIL* was positive (~0.35 MHz.ΔKp^{-1}), indicating that during the downward movement, the *ILs*' top frequency increased from its initial value. This increase in the frequency is expected since as the layer descends, it can suffer an additional increase of ionization arising from the metallic ions that contribute to the ion density in the ongoing sporadic Es layers. As the *ILs* presented a rise after 12:00-13:00 UT, the tendency was that the *ftIL* decreased with the increase of Kp_{av}, except during some intervals in June solstice. Analyzing the incoherent scatter data from the mid-latitude region of Arecibo, Rowe et al. (1974) observed an increase in the nighttime valley electron density during the occurrence of magnetic storms. They noted that in general, the integrated electron content of the lower valley region (130 km to 160 km) presented an increase with Kp index. Wakai (1967) reported a study about the maximum electron concentration of the nighttime E layer, the valley above it, and the appearance of the intermediate layer from analysis of the low-frequency ionogram obtained at Boulder on three nights of quiet, moderate, and severe geomagnetic activity. They observed an increase of the ionization in the nighttime valley at times of increased magnetic activity and the appearance of an intermediate layer in ~ 150 -160 km during periods of moderated activity. They also found that the height of the nocturnal intermediate layer became lower as the disturbances developed.

The effects of the magnetic storm on the intermediate layer were studied also by Rodger et al. (1981). Using ionosonde data over South Georgia, they showed that the rate of downward movement and the final height of the nocturnal intermediate layer is independent of the season or magnetic activity. They observed that the formation of an IL when the minimum virtual height of the F2 layer is above 220 km is very low, but can increase during magnetically disturbed periods. According to Rodger et al. (1981), no correlation was found between the IL's occurrence and magnetic activity. Such characteristics were also observed in the Brazilian sector. As shown by Santos et al. (2020), the *ILs*' occurrence over Cachoeira Paulista was very high both in 2009 (the same period of this report) and 2003. These results appear to show that the *ILs* occurrence could be independent of the magnetic disturbances, since the referred two periods of geomagnetic activity are totally different from each other. However, in agreement with the results present in Figure 5, the behavior of the ILs in terms of height and frequency can be affected as the magnetic activity increase.

Although the impacts of the geomagnetic activity on different layers of the ionosphere have been extensively studied, there is a lack of information about what happens in the ionospheric valley region during such conditions, mainly over the low and equatorial latitudes. Using the low-power VHF radar data over the equatorial site of Jicamarca, Chau and Kudeki (2006) showed that the 150-km echoes were not affected by the electric field reversal caused by a magnetic disturbance (Kp=5). As mentioned by them, a statistical study on the *ILs* occurrence based on the magnetic activity index Kp did not identify any correlation between magnetic activity and the 150-km echoes. On the other hand, our results show that a small variation in Kp_{av} index (~ 1.4) can affect the *ILs* over the low latitude sector over Brazil. Although the techniques used by us are different from those used by Chau and Kudeki (2006), the contrasting result reveals that the ionospheric valley is a complex region and additional studies need to be performed in order to understand the physical mechanism governing the generation of the intermediate layers during the occurrence of magnetic disturbances. It is important to emphasize that for the first time have been shown that a small variation in Kp_{av} index (by ~ 1.4) was able to impact the dynamics of the intermediate layer over the low latitude region during this period of deep solar minimum.

Acknowledgments: AMS thanks the financial support from FAPESP (process number: 2015/25357-4). The Digisonde data can be downloaded in Zenodo (identified as CAJ2M 2009 in https://doi.org/10.5281/zenodo.3967542). The Kp index was obtained from the World Data Center for Geomagnetism, Kyoto (http://wdc.kugi.kyoto-u.ac.jp/index.html). ISB thanks CNPq grant numbers 306844/2019-2 and 405555/2018-0. One of us (JHAS) had Grant number 303383/2019-4 from the Conselho Nacional de Desenvolvimento Cientifico e Tecnológico (CNPq). J. R. Souza would like to thank the CNPq (grant 307181/2018-9) for research productivity sponsorship and the INCT GNSS-NavAer supported by CNPq (465648/2014-2), FAPESP (2017/50115-0) and CAPES (88887.137186/2017-00). The Arecibo Observatory is operated by the University of Central Florida under a cooperative agreement with the National Science Foundation (AST-1744119) and in alliance with Yang Enterprises and Ana G. Méndez-Universidad Metropolitana.

5. References.

Balan, N., C. Y. Chen, J. Y. Liu, and G. J. Bailey (2012), Behavior of the low latitude ionosphere-thermosphere system at long deep solar minimum, Indian J. Radio Space Phys., 41, 89– 97.

Brum, C. G. M., F. S. Rodrigues, P. T. dos Santos, A. C. Matta, N. Aponte, S. A. Gonzalez, and E. Robles (2011), A modeling study of foF2 and hmF2 parameters measured by the Arecibo incoherent scatter radar and comparison with IRI model predictions for solar cycles 21, 22, and 23, J. Geophys. Res., 116, A03324, doi:10.1029/2010JA015727.

Brum, C. G. M., C. A. Tepley, J. T. Fentzke, E. Robles, P. T. dos Santos, and S. A. Gonzalez (2012), Long-term changes in the thermospheric neutral winds over Arecibo: Climatology based on over three decades of Fabry-Perot observations, J. Geophys. Res., 117, A00H14, doi:10.1029/2011JA016458.

Chau, J. L. and Kudeki, E.: Statistics of 150-km echoes over Jicamarca based on low-power VHF observations, Ann. Geophys., 24, 1305–1310, https://doi.org/10.5194/angeo-24-1305-2006, 2006.

Coley, W. R., R. A. Heelis, M. R. Hairston, G. D. Earle, M. D. Perdue, R. A. Power, L. L. H. B. J. Holt, and C. R. Lippincott (2010), Ion temperature and density relationships measured by CINDI from the C/NOFS spacecraft during solar minimum, J. Geophys. Res., 115, A02313, doi:10.1029/2009JA014665.

Dos Santos, Â. M., Batista, I. S., Abdu, M. A., Sobral, J. H. A., Souza, J. R., & Brum, C. G. M. (2019). Climatology of intermediate descending layers (or 150 km echoes) over the equatorial and low-latitude regions of Brazil during the deep solar minimum of 2009. Annales Geophysicae, 37(6), 1005–1024. https://doi.org/10.5194/angeo-37-1005-2019.

Echer, E., B. T. Tsurutani, and W. D. Gonzalez (2012), Extremely low geomagnetic activity during the recent deep solar cycle minimum, Proc. Int. Astron. Union, 7, 200–209, doi:10.1017/S174392131200484X.

Emmert, J. T., J. L. Lean, and J. M. Picone (2010), Record-low thermospheric density during the 2008 solar minimum, Geophys. Res. Lett., 37, L12102, doi:10.1029/2010GL043671.

Goncharenko, L. P., V.W. Hsu, C. G. M. Brum, S.-R. Zhang, and J. T. Fentzke (2013), Wave signatures in the midlatitude ionosphere during a sudden stratospheric warming of January 2010, J. Geophys. Res.: Space Physics, 118, doi:10.1029/2012JA018251.

Hady, A. A. (2013), Deep solar minimum and global climate changes. Journal of Advanced Research, V4, I3, P.209-214. doi:10.1016/j.jare.2012.11.001.

Heelis, R. A., W. R. Coley, A. G. Burrell, M. R. Hairston, G. D. Earle, M. D. Perdue, R. A. Power, L. L. H. B. J. Holt, and C. R. Lippincott (2009), Behavior of the O+/H+ transition height during the extreme solar minimum of 2008, Geophys. Res. Lett., 36, L00C03, doi:10.1029/2009GL038652.

525 Klenzing, J., F. A. Simoes, S. Ivanov, R. A. Heelis, D. Bilitza, R. F. Pfaff, and D. Rowland
526 (2011), Topside equatorial ionospheric density and composition during and after
527 extreme solar minimum, J. Geophys. Res., 116, A12330, doi:10.1029/2011JA017213.

528 Kutiev I, Tsagouri I, Perrone L, Pancheva D, Mukhtarov P, Mikhailov A, Lastovicka J,
529 Jakowski N, Buresova D, Blanch E, Andonov B, Altadill D, Magdaleno S, Parisi M &
530 Miquel Torta J (2013), Solar activity impact on the Earth's upper atmosphere. J.Space
531 Weather Space Clim., 3, A06, doi:10.1051/swsc/2013028.

532 Liu, J., L. Liu, B. Zhao, Y. Wei, L. Hu, and B. Xiong (2012), High-speed stream impacts
533 on the equatorial ionization anomaly region during the deep solar minimum year 2008,
534 J. Geophys. Res., 117, A10304,

535 Reinisch, B. W.: New techniques in ground-based ionospheric sounding and studies,
536 Radio Sci., 21, 331–341, 1986.

537 Rodger, A. S., Fitzgerald, P. H., and Broom, S. M.: The nocturnal intermediate layer over
538 South Georgia, J. Atmos. Terr. Phys., 43,1043–1050, 1981.

539 Rowe, F. J., Jr., Magnetic activity variations of the nighttime E region at Arecibo, Radio
540 Sci., 9, 175, 1974.

541 Santos, A. M., M. A. Abdu, J. R. Souza, J. H. A. Sobral, and I. S. Batista (2016),
542 Disturbance zonal and vertical plasma drifts in the Peruvian sector during solar
543 minimum phases, J. Geophys. Res. Space Physics, 121, doi:10.1002/2015JA022146.

544 Santos, A. M., Batista, I. S., Sobral, J. H. A., Brum, C. G. M., Abdu, M. A., & Souza, J.
545 R. (2020). Some differences in the dynamics of the intermediate descending layers
546 observed during periods of maximum and minimum solar flux. Journal of Geophysical
547 Research: Space Physics, 125, e2019JA027682.
548 https://doi.org/10.1029/2019JA027682.

549 Santos, Â. M., Batista, I. S., Brum, C. G. M., Sobral, J. H. A., Abdu, M. A., Souza, J. R.,
550 &. (2021). F region electric field effects on the intermediate layer dynamics during the
551 evening prereversal enhancement at equatorial region over Brazil. Journal of
552 Geophysical Research: Space Physics.

553 Scherliess, L., and B. G. Fejer (1997), Storm time dependence of equatorial disturbance
554 dynamo zonal electric fields, J. Geophys. Res., 102, 24,037–24,046,
555 doi:10.1029/97JA02165.

556 Souza, J.R., Brum, C.G.M., Abdu, M.A., Batista, I.S., Asevedo, W.D., Bailey, G.J.,
557 Bittencourt, J.A. (2010), Parameterized Regional Ionospheric Model and a comparison
558 of its results with experimental data and IRI representations, *Advances in Space*
559 *Research*, 46, 1032-1038, https://doi.org/10.1016/j.asr.2009.11.025.

560 Sreeja, V., T. K. Pant, L. Jose, and S. Ravindran (2011), Westward electric field
561 penetration to the dayside equatorial ionosphere during the main phase of the
562 geomagnetic storm on 22 July 2009, J. Geophys. Res., 116, A03303,
563 doi:10.1029/2010JA016013.

564 Terra, P., Vargas, F., Brum, C. G. M., & Miller, E. S. (2020). Geomagnetic and solar
565 dependency of MSTIDs occurrence rate: A climatology based on airglow observations

566 from the Arecibo Observatory ROF. Journal of Geophysical Research: Space Physics,
567 125, e2019JA027770. https://doi.org/10.1029/2019JA027770

568 Zerbo J.L., Amory-Mazaudier C., Ouattara F., 2013. Geomagnetism during solar cycle
569 23: Characteristics. J. Adv. Res, 4(3), 265–274. doi:10.1016/j.jare.2013.08.010.

570 Wakai, N. (1967), Quiet and disturbed structure and variations of the nighttime E-region,
571 J. Geophys. Res.,72, 4507-4517.

572 Wrenn, G., Rodger, A. S., & Rishbeth, H. (1987). Geomagnetic storms in the Antarctic
573 F-region. I. Diurnal and seasonal patterns for main phase effects. Journal of
574 Atmospheric and Solar-Terrestrial Physics, 49(9), 901–913.
575 https://doi.org/10.1016/0021-9169(87)90004-3

576 Yue, X., W. S. Schreiner, J. Lei, C. Rocken, Y. Kuo, and W. Wan (2010), Climatology
577 of ionospheric upper transition height derived from COSMIC satellites during the solar
578 minimum of 2008, J. Atmos. Terr. Phys., 72, 1270–1274,
579 doi:10.1016/j.jastp.2010.08.018.